

## A NEW MEASUREMENT OF THE COSMIC MICROWAVE BACKGROUND RADIATION TEMPERATURE AT $z = 1.97^1$

JIAN GE, JILL BECHTOLD, AND JOHN H. BLACK  
Steward Observatory, University of Arizona, Tucson, AZ 85721  
Received 1995 June 13; accepted 1996 July 18

### ABSTRACT

We present detections of absorption from the ground state and excited states of C I in the  $z = 1.9731$  damped Ly $\alpha$  system of the QSO 0013–004. The excitation temperature between the  $J = 0$  and  $J = 1$  fine-structure levels of C I is  $11.6 \pm 1.0$  K. We estimate other contributions to the excitation of the C I fine-structure levels, and use the population ratio of the excited state to the ground state to derive an estimate for the cosmic microwave background radiation (CMBR) temperature of  $T = 7.9 \pm 1.0$  K at 0.61 mm and  $z = 1.9731$ , which is consistent with the predicted value of  $T = 8.105 \pm 0.030$  K from the standard cosmology.

*Subject headings:* cosmic microwave background — quasars: absorption lines —  
quasars: individual (QSO 0013–004)

### 1. INTRODUCTION

The standard Friedmann cosmology predicts a simple relationship between the temperature of the cosmic microwave background radiation (CMBR) and redshift  $z$ :

$$T_{\text{CMBR}}(z) = T_{\text{CMBR}}(0)(1 + z), \quad (1)$$

where  $T_{\text{CMBR}}(0)$  is the CMBR temperature today (e.g., Peebles 1993). The present-day CMBR temperature has been measured precisely with the FIRAS instrument on the *Cosmic Background Explorer (COBE)*, with  $T_{\text{CMBR}}(0) = 2.726 \pm 0.010$  K (at the 95% confidence level; Mather et al. 1994).

The CMBR temperature at higher redshifts can be measured indirectly by using atomic fine-structure transitions in absorbers toward high-redshift quasars (Bahcall & Wolf 1968). The first attempt to measure the CMBR temperature in this way gave an upper limit of  $T_{\text{CMBR}} < 45$  K at  $z = 2.309$  from limits on the fine-structure excitation of C II toward PHL 957 (Bahcall, Joss, & Lynds 1973). Compared to other abundant species (such as O I, C II, Si II, and N II), C I is a better species to use because it has the smallest energy separations in its fine-structure levels. The ground term of C I is split into three levels ( $J = 0, 1$ , and  $2$ ) with  $J = 0-1$  and  $J = 1-2$  separations of 23.6 and 38.9 K (or 0.61 and 0.37 mm). Meyer et al. (1986) used the C I fine-structure lines of a damped Ly $\alpha$  system in the spectrum of QSO 1331+170 to obtain an upper limit ( $2\sigma$ ) of  $T_{\text{CMBR}} < 16$  K at  $z = 1.776$ . More recently, Songaila et al. (1994b) have observed QSO 1331+170 again and obtained  $T_{\text{CMBR}} = 7.4 \pm 0.8$  K, which agrees with the predicted value of 7.58 K. C II is another good species to use for the CMBR measurements at high redshift because it has a reasonably small energy separation between its fine-structure levels, 91.3 K. Songaila et al. (1994a) obtained a  $2\sigma$  upper limit of  $T_{\text{CMBR}} < 13.5$  K at  $z = 2.909$  toward QSO 0636+680 based on upper limits to C II fine structure. Lu et al. (1995) achieved a  $3\sigma$  upper limit of  $T_{\text{CMBR}} < 19.6$  K at  $z = 4.3829$  toward QSO 1202–07 by measuring upper limits for the excited states of C II.

There are several difficulties in carrying out measurements of  $T_{\text{CMBR}}(z)$  with quasar absorbers. First, the ground-state C I absorption lines are often weak and difficult to detect in quasar absorbers at high redshift. Second, other noncosmological sources such as collisions and pumping by UV radiation can also populate the excited fine-structure levels of C I. Thus, the excitation temperature derived is an upper limit to the CMBR temperature, unless the local excitation can be estimated. Third, most absorption lines from abundant species such as O I, C II, Si II, N II show strong saturation in their ground state transitions, and, hence, the population ratio of their excited state to the ground state cannot be accurately determined.

In this paper we present spectra obtained at the Multiple Mirror Telescope (MMT) of C I and C I\* absorption in the  $z = 1.9731$  damped Ly $\alpha$  system toward the QSO 0013–004 and estimate the contributions of the various sources of excitation. The neutral hydrogen column density of the  $z = 1.9731$  damped system is  $N(\text{H I}) = (5 \pm 1) \times 10^{20} \text{ cm}^{-2}$  (Pettini et al. 1994). The metal abundance is about one-fourth of the solar value, and the heavy-element depletion by dust is more than 20% of the Milky Way value (Pettini et al. 1994). These properties suggested to us that this system was a good candidate for a search for C I absorption.

### 2. OBSERVATIONS

The observations of QSO 0013–004 were obtained on 1994 October 9 and December 8 with the Blue Channel Spectrograph and the Loral 3072  $\times$  1024 CCD on the MMT. The 832 line  $\text{mm}^{-1}$  grating was used in second order. A  $\text{CuSO}_4$  filter was used to block the first-order light. In October, we took four exposures, three 50 minute and one 60 minute, with wavelength coverage from 3860 to 4960 Å. Because of poor seeing conditions, a  $1.5 \times 180''$  slit was used to obtain a spectral resolution of 1.3 Å (FWHM). In December, we took four 50 minute exposures with wavelength coverage from 4380 to 5459 Å. A  $1'' \times 180''$  slit was used to obtain a spectral resolution of 1 Å (FWHM). In all our observations, the quasar was moved a few arcseconds along the slit between each exposure to smooth out any residual irregularities in the detector response which remained after flat-fielding. An exposure of a He-Ne-Ar lamp and a quartz lamp was taken before and after each

<sup>1</sup> Observations here were obtained with the Multiple Mirror Telescope, a joint facility of the University of Arizona and the Smithsonian Institution.

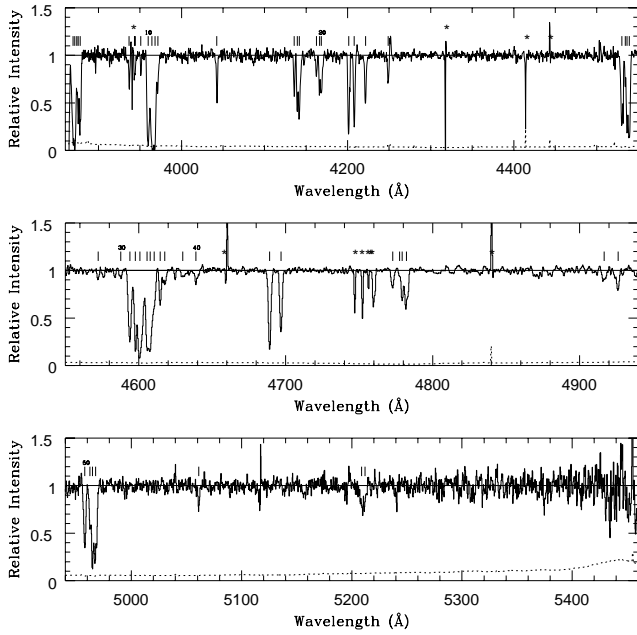


FIG. 1.—Spectrum of QSO 0013—004 with significant absorption lines marked. The solid line is the fit to the continuum. The dotted line is the  $1\sigma$  error. Features marked with an asterisk are bad columns or traps in the CCD.

exposure of the object to provide an accurate wavelength reference, a measure of the instrumental resolution, and a flat-field correction. The spectra were reduced using standard routines in IRAF and were summed with individual exposures weighted by the signal-to-noise ratio (S/N). We then summed the spectra with the wavelength coverage from 4550 to 5940 Å from our two runs to reach S/N of about 40.

Figure 1 shows the total spectrum obtained. All reported wavelengths are in vacuum and have been corrected to the heliocentric frame. The continuum was fitted, and significant absorption features were identified and measured in the way described by Bechtold (1994). The spectra shown were normalized by their fitted continuum. All absorption lines with more than  $5\sigma$  significance are marked. Table 1 shows the equivalent widths of the absorption lines and their identifications. The equivalent widths were measured by specifying start and stop wavelengths for each absorption feature by hand (cf. Bechtold 1994). The central wavelength of each line is the centroid, weighted by the depth of each pixel in the line profile below the continuum. The error for the central wavelength shown in this table is from the uncertainty in the measurement of the equivalent width. There are at least four velocity components associated with the  $z = 1.9731$  damped system. The redshifts are  $z = 1.9673$ ,

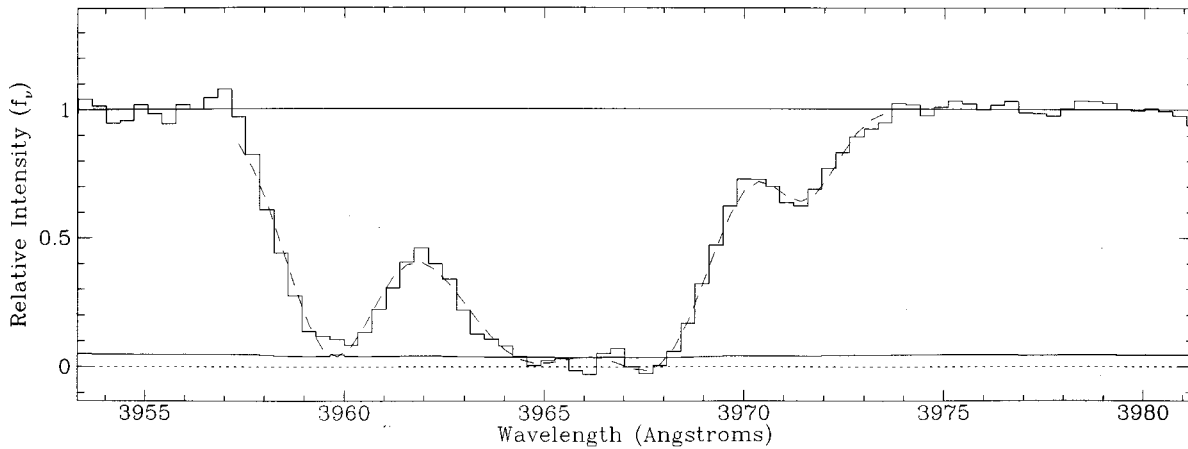


FIG. 2a

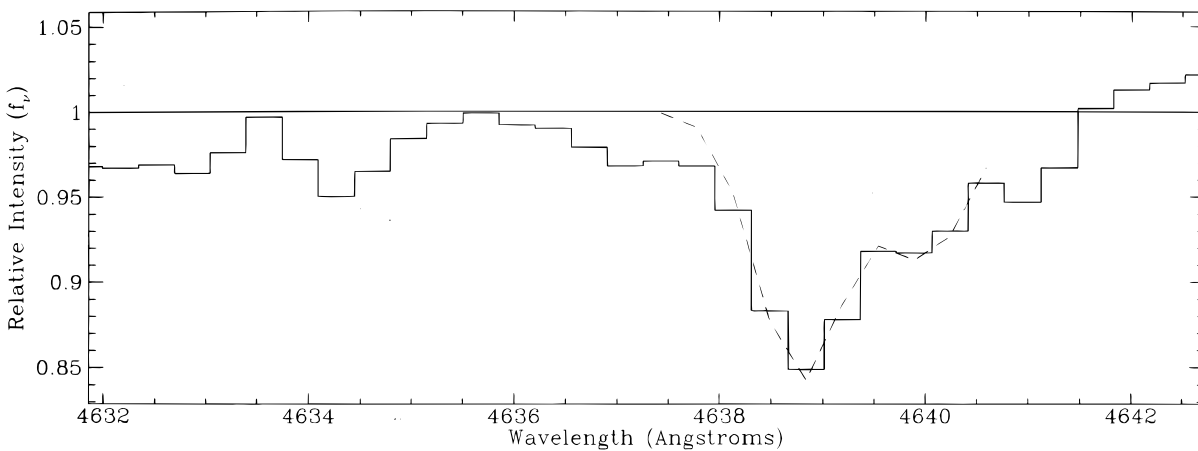


FIG. 2b

FIG. 2.—(a) Profile fit to the C II lines at  $z = 1.9672$ , 1.9711, and 1.9733, and C II\* line at  $z = 1.9732$ . The solid line is the continuum. The dashed line is the Gaussian fit to the absorption lines with four velocity components (see Table 1 and text). (b) Profile fit to the C I  $\lambda 1560.31$  and C I\*  $\lambda 1560.68$ , 1560.70 lines at  $z = 1.9731$ . The solid line is the continuum. The dashed line is the Gaussian fit to the absorption lines.

TABLE 1  
IDENTIFICATIONS OF ABSORPTION LINES OF QSO 0013–004

Number	$\lambda_{\text{obs}}$ (Å)	$\sigma(\lambda)$	$W_{\text{obs}}$ (Å)	$\sigma(W)$	$W_{\text{obs}}^a$ (Å) <sup>a</sup>	$\sigma(W)^a$	Significance Level	Identification	$z_{\text{abs}}$
1	3869.22	0.03	2.145	0.081	...	...	26.62	O I 1302	1.9714
2	3871.58	0.03	2.719	0.093	...	...	29.28	O I 1302	1.9732
								Si II 1304	1.9673
3	3874.02	0.03	0.537	0.057	...	...	9.41	Si II 1304	1.9700
								O I 1302	1.9756
4	3875.63	0.04	1.336	0.074	1.22	0.23	18.16	Si II 1304	1.9713
								O I 1302	1.9776
5	3878.03	0.05	1.974	0.086	2.12	0.22	22.31	Si II 1304	1.9731
6	3936.93	0.09	0.564	0.055	...	...	10.32	C IV 1548	1.5429
7	3943.25	0.05	0.286	0.037	...	...	7.79	C IV 1550	1.5428
8	3944.27	0.09	0.257	0.041	...	...	6.23	O I 1304	2.0290
9	3951.09	0.08	0.252	0.040	...	...	6.28	Si II 1304	2.0291
								C I 1329	1.9731
10	3959.78	0.02	2.853	0.051	2.91	0.19	55.44	C II 1334	1.9672
11	3964.48	0.02	4.581	0.052	4.80	0.70	88.57	C II 1334	1.9711
12	3967.95	0.02	2.664	0.042	2.31	0.58	63.68	C II 1334	1.9733
13	3971.34	0.05	0.797	0.045	0.80	0.09	17.81	C II* 1335	1.9732
14	4042.49	0.06	0.855	0.046	...	...	18.54	C II 1334	2.0292
15	4135.63	0.07	0.730	0.046	...	...	15.80	Si IV 1393	1.9674
16	4139.41	0.03	1.137	0.039	...	...	29.10	Si IV 1393	1.9700
17	4141.78	0.02	1.577	0.041	...	...	38.54	Si IV 1393	1.9717
18	4162.39	0.10	0.406	0.043	...	...	9.34	Si IV 1402	1.9673
19	4166.10	0.04	0.654	0.039	...	...	16.99	Si IV 1402	1.9699
20	4168.29	0.04	1.031	0.043	...	...	23.97	Si IV 1402	1.9715
21	4201.21	0.02	1.961	0.040	...	...	48.43	C IV 1548	1.7136
22	4208.07	0.03	1.610	0.043	...	...	37.07	C IV 1402	1.7135
23	4221.58	0.03	1.045	0.036	...	...	29.02	Si IV 1393	2.0289
24	4248.90	0.08	0.578	0.044	...	...	13.20	Si IV 1402	2.0290
25	4530.40	0.02	1.980	0.043	...	...	46.48	Si II 1526	1.9674
26	4534.19	0.06	0.478	0.038	...	...	12.53	Si II 1526	1.9699
27	4536.38	0.02	1.754	0.038	1.89	0.14	46.13	Si II 1526	1.9714
28	4538.98	0.02	2.486	0.042	2.55	0.14	66.14	Si II 1526	1.9731
29	4572.32	0.11	0.146	0.026	...	...	5.59	...	...
30	4587.70	0.16	0.158	0.031	...	...	5.11	...	...
31	4594.00	0.03	1.880	0.037	...	...	51.47	C IV 1548	1.9673
32	4597.70	0.02	1.746	0.030	...	...	58.65	C IV 1548	1.9697
33	4601.13	0.02	3.724	0.039	...	...	95.74	C IV 1548	1.9719
34	4605.54	0.01	1.804	0.027	...	...	66.51	C IV 1550	1.9698
35	4608.24	0.01	2.396	0.031	...	...	77.52	C IV 1550	1.9716
								C IV 1548	1.9756
36	4610.95	0.04	0.515	0.026	...	...	19.60	C IV 1550	1.9733
								C IV 1548	1.9777
37	4614.64	0.05	0.592	0.032	...	...	18.45	C IV 1550	1.9757
38	4617.95	0.08	0.250	0.029	...	...	8.72	C IV 1550	1.9778
39	4630.00	0.015	0.162	0.030	...	...	5.31	C I 1560	1.9674
40	4638.81	0.08	0.198	0.026	0.17	0.02	7.57	C I 1560	1.9730
41	4689.12	0.03	1.760	0.036	...	...	49.04	C IV 1548	2.0288
42	4696.79	0.03	1.292	0.032	...	...	40.91	C IV 1550	2.0287
43	4772.77	0.06	0.372	0.018	...	...	20.73	Fe II 1608	1.9673
44	4777.48	0.06	0.074	0.011	...	...	7.04	Fe II 1608	1.9702
45	4779.34	0.02	0.548	0.013	...	...	41.00	Fe II 1608	1.9714
46	4782.21	0.02	0.992	0.016	...	...	60.25	Fe II 1608	1.9731
47	4916.83	0.21	0.321	0.047	...	...	6.77	C I 1656	1.9674
48	4926.08	0.10	0.432	0.043	0.44	0.05	10.13	C I 1656	1.9730
49	4957.65	0.05	1.531	0.066	...	...	23.29	Al III 1670	1.9673
50	4962.44	0.08	0.923	0.062	...	...	14.83	Al III 1670	1.9701
51	4964.81	0.02	1.753	0.048	...	...	36.25	Al III 1670	1.9715
52	4967.65	0.05	2.232	0.067	...	...	33.11	Al III 1670	1.9732
53	5061.16	0.15	0.425	0.061	...	...	6.94	Al III 1670	2.0292
54	5208.79	0.16	0.735	0.091	...	...	8.12	...	...
55	5211.96	0.17	0.523	0.085	...	...	6.16	...	...

<sup>a</sup> The equivalent widths are measured through Gaussian profile fitting.

1.9700, 1.9714, and 1.9731. Two components ( $z = 1.9673, 1.9731$ ) clearly show absorption lines from the C I ground-state levels. Since some important lines, such as C II  $\lambda 1334$  and C I  $\lambda 1560$ , are blended lines, we have also tried to fit the absorption lines with Gaussians. This method is similar to that described by Schneider et al. (1993). The equivalent

widths measured in this way are consistent with those listed in Table 1 within  $1\sigma$  errors even for heavily blended absorption lines. Figure 2 shows the Gaussian fits for the C II  $\lambda 1334$  line and C I  $\lambda 1560$  line at  $z = 1.97$ .

Table 2 lists the rest wavelengths, predicted wavelengths, and  $f$ -values for the two strongest C I multiplets and the

TABLE 2  
EXPECTED WAVELENGTHS FOR C I AND C II IN THE  $z = 1.9731$  ABSORBER

Multiplet	$J$	$\lambda_{\text{rgst}}$ (Å)	$\lambda_{\text{rest}}(1+z)^a$ (Å)	$f$	$W_{\text{obs}}$ (Å)	$\sigma(W)$	SL
C I multiplet 2 .....	0	1656.928	4926.213	0.141	0.432	0.043	10.1
	1	1656.267	4924.247	0.059	0.088	0.027	3.3
	1	1657.379 <sup>b</sup>	4927.554	0.035	...	...	...
	1	1657.907	4929.123	0.047	0.054	0.028	1.9
	2	1657.008 <sup>b</sup>	4926.451	0.105	...	...	...
	2	1658.121 <sup>c</sup>	4929.594	0.035	<0.111	...	...
C I multiplet 3 .....	0	1560.309	4638.955	0.080	0.198(0.17) <sup>f</sup>	0.026(0.02) <sup>f</sup>	7.6
	1	1560.682	4639.908	0.060	0.082(0.09) <sup>f</sup>	0.019(0.02) <sup>f</sup>	4.4
	1	1560.709 <sup>d</sup>	4640.144	0.020	...	...	...
	2	1561.340 <sup>e</sup>	4642.020	0.012	<0.087	...	...
	2	1561.367 <sup>e</sup>	4642.100	0.001	<0.087	...	...
	2	1561.438 <sup>e</sup>	4642.311	0.068	<0.087	...	...
C II multiplet 1 .....	1/2	1334.532	3967.698	0.128	2.664	0.039	68.23
	3/2	1335.663 <sup>e</sup>	3971.059	0.013	...	...	...
	3/2	1335.708	3971.193	0.115	0.797	0.042	18.92

<sup>a</sup> These wavelengths are vacuum, heliocentric values.

<sup>b</sup> The line is blended with  $J = 0$  line of  $\lambda 1656.928$ .

<sup>c</sup> The upper limits are  $3\sigma$ .

<sup>d</sup> The line is blended with  $J = 1$  line of  $\lambda 1560.709$ .

<sup>e</sup> The line is blended with  $J = 3/2$  line of  $\lambda 1335.708$ .

<sup>f</sup> The measurement in parentheses is from the Gaussian profile fitting.

strongest C II multiplet in the  $z = 1.9731$  component. The  $f$ -values are from the compilation of Morton (1991). We also list the observed equivalent widths of these lines. Figure 3 shows our spectrum of QSO 0013–004 in the vicinity of the two C I multiplets and one C II multiplet listed in Table 2. The fit of the continuum and the  $1\sigma$  deviation of each pixel are also displayed. C I  $J = 0$  absorption lines are clearly present in UV multiplet 2 at 1656.93 Å and multiplet 3 at 1560.31 Å. C II  $J = 1/2$  (1334.53 Å) and  $J = 3/2$  (1335.70 Å) absorption lines of multiplet 1 are also present. C I  $J = 1$  absorption is present in the multiplet 2 at 1656.27 and 1657.91 Å and multiplet 3 at 1560.68 Å. The C I and C II

lines are observed at the wavelengths expected from the redshift of other low-ionization ions, such as Zn II (Pettini et al. 1994), Fe II, and Si II (Table 1), within the wavelength uncertainty of about 0.1 Å. The C I  $J = 0$  absorption line at 1656.928 Å is blended with one of the C I  $J = 1$  lines at 1657.379 Å and also one of the C I  $J = 2$  lines at 1657.008 Å. No absorption features for  $J = 2$  at 1658.121 Å and 1561.340, 1561.367, and 1561.438 Å are detected. The third strongest C I multiplet at 1329 Å is blended with Si II  $\lambda 1304$  from another absorber at  $z = 2.0290$ .

### 3. RESULTS

We can use the relative population ratios of the  $J = 1$  and  $J = 0$  levels in the multiplets 2 and 3 to obtain the excitation temperature of the C I fine-structure levels in its ground state and to derive limits on the CMBR temperature at  $z = 1.9731$ . Since our spectral resolution is insufficient to resolve the profiles of the lines, we used observed Si II lines, at 1260, 1304, 1526 and 1808 Å, to construct an empirical curve of growth (Fig. 4). The measurement of Si II  $\lambda 1206$  is from another observation by Bechtold, who found a rest-frame equivalent width for this

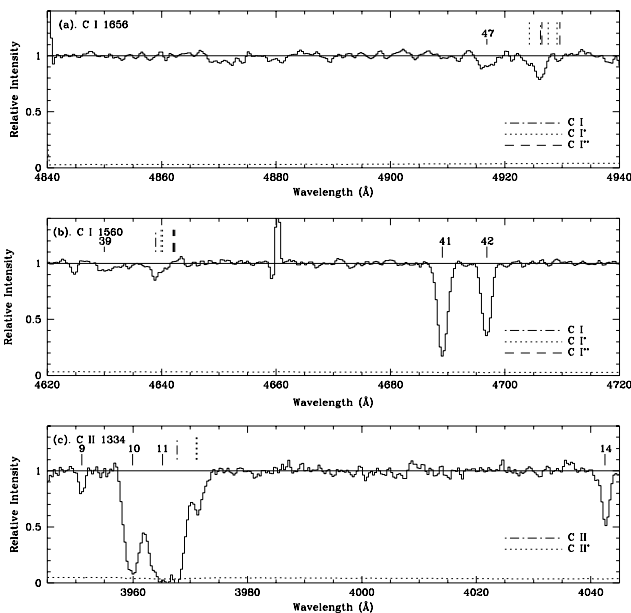


FIG. 3.—Spectrum of QSO 0013–004 showing the C I multiplets 2 and 3 and C II multiplet 1 listed in Table 1. The dotted line shows the  $1\sigma$  error. The expected positions of the ground state ( $J = 0$  or  $1/2$ ) and excited states ( $J = 1, 2$ , or  $3/2$ ) are marked.

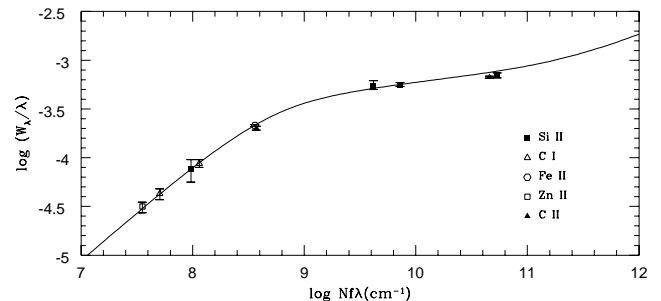


FIG. 4.—Curve of growth for singly ionized and neutral species in the  $z = 1.9731$  system. The solid line which best fits the data from Si II  $\lambda$  absorption lines is the theoretical curve of growth for  $b = 42 \pm 2 \text{ km s}^{-1}$ .

line of  $0.8691 \pm 0.0188 \text{ \AA}$ . The Si II curve of growth provides a Doppler parameter  $b = 42 \pm 2 \text{ km s}^{-1}$  which we then used to infer the column densities of different absorption lines. The results of calculated column densities are shown in Table 3. We have also shown central optical depths for different C I and C II lines. The central optical depths for C I and C I\* absorption lines indicate that all these lines are on the linear part of the curve of growth. Thus, the derived column densities for the C I fine-structure levels are independent of the derived  $b$  value. However, the optical depths for the C II and C II\* lines indicate that they are saturated, and so the derived column densities for the C II and C II\* lines depend on the  $b$ -value. The derived  $b$ -value indicates that there are probably several velocity components blended with each other. However, the uncertainties in the column densities from single  $b$ -value curve-of-growth analyses are usually on the order of a factor of 2 (Jenkins 1986). We therefore use this  $b$ -value to derive the column densities for the saturated C II and C II\* lines. In our calculation, because of our limited resolution, we have combined the  $f$ -values of the two  $J = 1$  lines of C I multiplet 3,  $\lambda\lambda 1560.682, 1560.709$ , and also the  $f$ -values of the two  $J = 3/2$  lines of C II multiplet 1,  $\lambda\lambda 1335.663, 1335.708$ , and further derived the relative population ratios of their fine-structure levels. We have assumed that the absorption at  $4926.313 \text{ \AA}$  is only from the  $J = 0, 1656.928 \text{ \AA}$  of C I multiplet 2 since the strengths of other blended lines such as  $J = 1, 1657.379 \text{ \AA}$  and  $J = 2, 1657.008 \text{ \AA}$  are much weaker than that of the  $J = 0$  line. The other two  $J = 1$  lines of C I multiplet 2,  $\lambda\lambda 1656.267, 1657.907$ , are detected at about the  $2\text{--}3 \sigma$  level and, in the weighted mean, are present at the  $4 \sigma$  level. We therefore have used this weighted mean to derive the population ratio of the  $J = 1$  and  $J = 0$  levels of C I multiplet 2, as shown in Table 3.

Next, we can use the relative population ratios to derive the excitation temperature of the C I and C II fine-structure levels. According to the Boltzmann equation, an excitation

temperature  $T_{\text{ex}}$  can be expressed in terms of the column densities  $N_e$  and  $N_g$  in the excited and the ground-state levels,

$$N_e/N_g = g_e/g_g \exp(-\Delta E_{\text{eg}}/kT_{\text{ex}}), \quad (2)$$

where  $\Delta E_{\text{eg}}$  is the energy difference between the excited and ground levels.  $\Delta E_{\text{eg}}$  is 23.6 K for the difference between  $J = 1$  and  $J = 0$  in C I and 91.2 K for the difference between  $J = 3/2$  and  $J = 1/2$  in C II. The weights are  $g_j = 2J + 1$ . Thus, the population ratios  $N(J = 1)/N(J = 0)$  in the C I multiplets 2 and 3 indicate excitation temperatures  $T_{\text{ex}} = 11.6 \pm 1.6 \text{ K}$  and  $11.6 \pm 1.4 \text{ K}$  for multiplets 2 and 3, respectively. The weighted mean value is  $T_{\text{ex}} = 11.6 \pm 1.0 \text{ K}$  for the C I fine structure. The population ratio  $N(J = 3/2)/N(J = 1/2)$  of the C II fine-structure levels indicates an excitation temperature  $T_{\text{ex}} = 16.1 \pm 1.4 \text{ K}$ . Because the C I and C II fine-structure levels can be excited by not only the CMBR field but also other excitation sources such as collision and UV pumping, the derived excitation temperatures are upper limits to the CMBR temperature at  $z = 1.9731$ . Thus, the upper limits of the CMBR temperature at 0.61 and 0.16 mm are 11.6 and 16.1 K, respectively, consistent with the predicted value at this redshift,  $T_{\text{CMBR}} = 8.105 \text{ K}$ .

We can estimate the contribution from collisional and UV pumping to the excitation of C I by modeling the absorption region. The equilibrium between the excitation and de-excitation of the C I  $J = 0 \rightarrow 1$  fine structure can be expressed as

$$N_0 \left( \sum_j \langle \sigma_{01} v \rangle_j n_j + B_{01} I_\nu + \Gamma_{01} \right) = N_1 \left( A_{10} + B_{10} I_\nu + \sum_j \langle \sigma_{10} v \rangle_j n_j + \Gamma_{10} \right), \quad (3)$$

where  $j = \text{H}, e, p, \text{He}, \text{and } \text{H}_2$ ,  $\Gamma_{10}$  is the UV pumping rate from  $J = 0$  to  $J = 1$ , and the  $\Gamma_{01}$  is the UV pumping rate from  $J = 1$  to  $J = 0$ . The spontaneous transition probability for the C I  $J = 1 \rightarrow 0$  transition is  $A_{10} = 7.93 \times 10^{-8} \text{ s}^{-1}$  (Bahcall & Wolf 1968). The collisional excitation rates from different collision partners are given by Launay & Roueff (1977), Keenan et al. (1986), Johnson, Burke, & Kingston (1987), Roueff & Le Bourlet (1990), Flower (1990), Staemmler & Flower (1991), and Schröder et al. (1991). The collisional de-excitation rate is given by

$$\langle \sigma_{10} v \rangle_j = \frac{1}{3} \langle \sigma_{01} v \rangle_j \exp(23.6 \text{ K}/T_k), \quad (4)$$

for  $j = \text{H}, e, p, \text{He}, \text{and } \text{H}_2$ .  $B_{10} = \frac{1}{3} B_{01}$ . The  $J = 0 \rightarrow 1$  excitation rate due to the absorption of the CMBR,  $B_{01}$ , can be expressed as

$$I_\nu B_{01} = 2.38 \times 10^{-7} / [\exp(23.6 \text{ K}/T_{\text{CMBR}}) - 1] \text{ s}^{-1}. \quad (5)$$

The UV pumping rate depends on the strength of UV radiation field.  $\Gamma_{01} = 7.55 \times 10^{-10} \text{ s}^{-1}$  and  $\Gamma_{10} = 2.52 \times 10^{-10} \text{ s}^{-1}$  if the UV field intensity for  $z = 1.9731$  is the same as that in the Milky Way which is about  $4.7 \times 10^{-19} \text{ ergs s}^{-1} \text{ cm}^{-2} \text{ Hz}^{-1}$  at  $912 \text{ \AA}$  (Jenkins & Shaya 1979; Mathis et al. 1983).

In order to solve equation (3), we have to know  $n_{\text{H}}, n_e, n_{\text{He}}, n_{\text{H}_2}$ , and the UV pumping rates. To estimate plausible values for the  $z = 1.9731$  absorber we constructed a photoionization model with the CLOUDY program (Ferland 1993). For the input to CLOUDY, we adopted a metallicity of 25% of the solar value, i.e.,  $[\text{Zn}/\text{H}] = -0.61$ , for all the elements in the  $z = 1.9731$  damped system (Pettini et al.

TABLE 3

EXCITATION TEMPERATURE OF C I AND C II AT  $z = 1.9731$ 

Multiplet	Density	$\tau_0$
C I multiplet 2:		
$N(\times 10^{13} \text{ cm}^{-2})$ :		
$J = 0, \lambda = 1656.928 \text{ \AA} \dots\dots$	$4.9 \pm 0.5$	0.43
$J = 1, \lambda = 1656.267 \text{ \AA} \dots\dots$	$2.1 \pm 0.6$	0.078
$J = 1, \lambda = 1657.907 \text{ \AA} \dots\dots$	$1.6 \pm 0.8$	0.047
$\langle J = 1 \rangle_{\text{weighted}} \dots\dots\dots$	$1.9 \pm 0.5$	
$N(J = 1)/N(J = 0) \dots\dots\dots$	$0.39 \pm 0.11$	
$T_{\text{ex}} (\text{K}) \dots\dots\dots$	$11.6 \pm 1.6$	
C I multiplet 3:		
$N(\times 10^{13} \text{ cm}^{-2})$ :		
$J = 0, \lambda = 1560.309 \text{ \AA} \dots\dots$	$4.1 \pm 0.5$	0.19
$J = 1, \lambda = 1560.695 \text{ \AA} \dots\dots$	$1.6 \pm 0.4$	0.076
$N(J = 1)/N(J = 0) \dots\dots\dots$	$0.39 \pm 0.10$	
$T_{\text{ex}} (\text{K}) \dots\dots\dots$	$11.6 \pm 1.4$	
Weighted mean of C I multiplets:		
$N(J = 0)(\times 10^{13} \text{ cm}^{-2}) \dots\dots\dots$	$4.5 \pm 0.4$	
$N(J = 1)(\times 10^{13} \text{ cm}^{-2}) \dots\dots\dots$	$1.8 \pm 0.3$	
$N(J = 1)/N(J = 0) \dots\dots\dots$	$0.39 \pm 0.07$	
$T_{\text{ex}} (\text{K}) \dots\dots\dots$	$11.6 \pm 1.0$	
C II multiplet 1:		
$N(J = 1/2)(\times 10^{16} \text{ cm}^{-2}) \dots\dots$	$2.7 \pm 1.2$	164
$N(J = 3/2)(\times 10^{14} \text{ cm}^{-2}) \dots\dots$	$1.9 \pm 0.2$	1.1
$N(J = 3/2)/N(J = 1/2) \dots\dots\dots$	$7.0(\pm 3.2) \times 10^{-3}$	
$T_{\text{ex}} (\text{K}) \dots\dots\dots$	$16.1 \pm 1.4$	

1994). We have also considered depletion by dust grains. The dust-to-gas ratio is about 20% of the Milky Way, estimated from the relative depletion of Cr and Ni to Zn, i.e.,  $[\text{Cr}/\text{Zn}] \leq -1.15$  (Pettini et al. 1994) and  $[\text{Ni}/\text{Zn}] \leq -0.98$  from our data. For the shape of the spectral energy distribution (SED), we adopted a parameterization of the Milky Way SED given by Black (1987). Because we are interested in the low ionization species (C I, C II, and H<sub>2</sub>), the results are sensitive to the UV flux adopted at wavelengths from  $\sim 500$  to  $1100 \text{ \AA}$  which is probably dominated by local sources within the Galaxy. The adopted flux at the Lyman limit is about 1 order of magnitude higher than the metagalactic UV flux at  $z \approx 2$ , estimated to be  $J(912 \text{ \AA}) \approx 3.8 \times 10^{20} \text{ ergs s}^{-1} \text{ cm}^{-2} \text{ Hz}^{-1}$  (e.g., Bechtold 1994), so we have neglected the ionization contribution from the metagalactic radiation field. The results are shown in Figure 5. The ionization parameter,  $U = \phi(\text{H})/n_{\text{H}}c = 2.7 \times 10^{-4}$ , gives the best fit to the observational results, where  $\phi(\text{H})$  is the surface flux of hydrogen-ionizing photons ( $\text{cm}^{-2} \text{ s}^{-1}$ ). The photoionization model with this  $U$ -value indicates that the column density of molecular hydrogen,  $N(\text{H}_2) = 5 \times 10^{19} \text{ cm}^{-2}$ , or  $n_{\text{H}_2} = 0.1n_{\text{H}}$ ; the electron temperature  $T_e \sim 1 \times 10^3$ –80 K, and  $n_e/n_{\text{H}} \sim 1.0 \times 10^{-2}$ – $5 \times 10^{-4}$  from the outer region to the inner region of the absorber.  $T_e \sim 100$  K and  $n_e/n_{\text{H}} \sim 5.0 \times 10^{-4}$  dominate most regions of the cloud. In the following discussions we adopted two sets of extreme limit values:  $n_e/n_{\text{H}} = 1.0 \times 10^{-2}$  and  $T_e = 1000$  K, and  $n_e/n_{\text{H}} = 5.0 \times 10^{-4}$  and  $T_e = 100$  K.

In order to estimate  $n_{\text{H}}$  we use a value derived from the relative population ratio of the C II fine-structure levels. In the H I dominant region with  $n_{\text{H}} \lesssim 3 \times 10^3 \text{ cm}^{-3}$  (Flower 1990; Bahcall & Wolf 1968), the ratio of excited C II\* relative to the ground-state C II populations can be expressed as

$$\frac{N(\text{C II}^*)}{N(\text{C II})} \approx \frac{n_{\text{H}} \langle \sigma_{01} v \rangle_{\text{H}} + n_e \langle \sigma_{01} v \rangle_e + n_{\text{H}_2} \langle \sigma_{01} v \rangle_{\text{H}_2}}{A_{10}},$$

where  $A_{10} = 2.29 \times 10^{-6} \text{ s}^{-1}$  is the spontaneous transition probability; we have neglected the excitation term due to proton collisions because this term is much less than the others at  $T_e < 2 \times 10^5$  K (Bahcall & Wolf 1968). As a result,  $n_{\text{H}} = 21.0 \pm 9.6 \text{ cm}^{-3}$  when  $T_e = 100$  K, and  $n_{\text{H}} = 4.5 \pm 2.0 \text{ cm}^{-3}$  when  $T_e = 1000$  K. Thus, the H-ionization photon flux  $\phi(\text{H})$  is  $17.0 \times 10^7 \text{ cm}^{-2} \text{ s}^{-1}$  when  $T_e = 100$  K and  $3.6 \times 10^7 \text{ cm}^{-2} \text{ s}^{-1}$  when  $T_e = 1000$  K. For comparison,

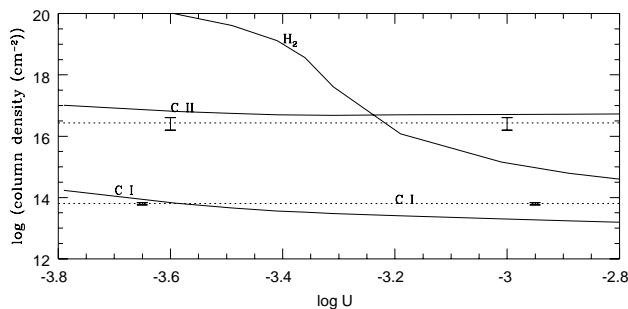


FIG. 5.—Results of ionization model for a H I dominant region with  $N(\text{H I}) = 5 \times 10^{20} \text{ cm}^{-2}$ . The ordinate is the column density of various ions, the abscissa is the log of ionization parameter  $U$ . The solid lines are predicted values from CLOUDY. The dotted lines correspond to measured column densities of C II and C I. The error bars are  $1 \sigma$  errors on the column densities of C I and C II which include errors from photon statistics and uncertainty in the  $b$  value ( $42 \pm 2 \text{ km s}^{-1}$ ).

the Milky Way H-ionization flux is about  $1 \times 10^7 \text{ cm}^{-2} \text{ s}^{-1}$  calculated from the SED given by Black (1987). Thus, the UV pumping rates in our calculations are 17.0 and 3.6 times the Milky Way rate for the 100 and 1000 K cases, respectively. We obtain  $n_e = 1.05 \times 10^{-2} \text{ cm}^{-3}$ ,  $n_{\text{He}} = 1.68 \text{ cm}^{-3}$ , and  $n_{\text{H}_2} = 2.1 \text{ cm}^{-3}$  for the  $T_e = 100$  K case and  $n_e = 4.5 \times 10^{-2} \text{ cm}^{-3}$ ,  $n_{\text{He}} = 0.36 \text{ cm}^{-3}$ , and  $n_{\text{H}_2} = 0.45 \text{ cm}^{-3}$  for the  $T_e = 1000$  K case.

Substituting into equation (4), we finally estimate the contribution to the excitation of the C I fine-structure levels from collisions and UV pumping. After these contributions are removed, the CMBR temperature at  $z = 1.9731$   $T_{\text{CMBR}} = 7.9 \pm 1.0$  K when  $T_e = 100$  K is adopted, and  $T_{\text{CMBR}} = 10.6 \pm 1.0$  K when  $T_e = 1000$  K is used. Since the electron temperature in most regions of the  $z = 1.9731$  absorber is around 100 K, our best guess for the CMBR temperature at  $z = 1.9731$  is  $7.9 \pm 1.0$  K.

The above results are based on the assumption of a single homogeneous zone model, which is probably different from the real case. Previous high-resolution observations of QSO 1331+170 have shown that the C I absorption lines split into two components with different excitation temperatures (Songaila et al. 1994b). There may be two or more different velocity components associated with C I absorption in the QSO 0013–004 system. Without knowledge of the individual cloud structure, there may be some uncertainties in the correction of local excitation from only considering the C II fine-structure excitation. Ultimately, a higher resolution spectrum is needed to get an improved measurement of the CMBR temperature at  $z = 1.9731$ .

#### 4. DISCUSSION

We have estimated the local contributions to the excitation of C I, which can contribute  $\sim 1$ –3 K to the excitation

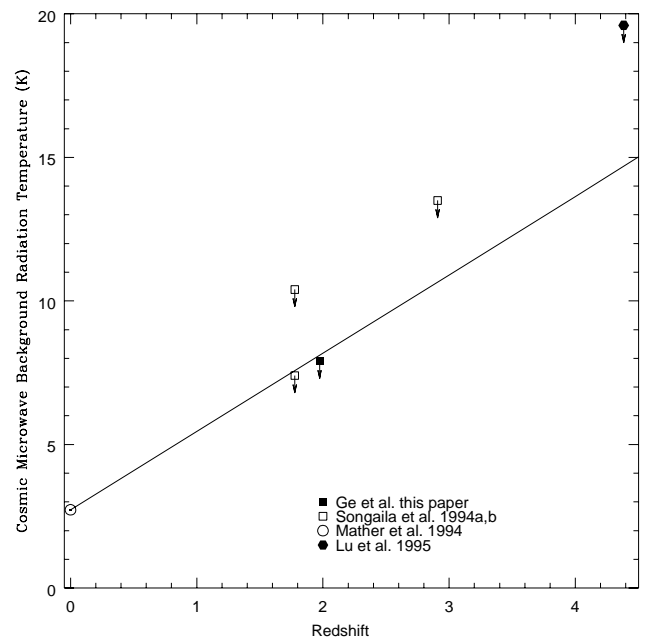


FIG. 6.—Measurements of the CMBR temperature as a function of redshifts. The solid line is the predicted relation. The filled circle is from the COBE measurement (Mather et al. 1994). The open squares are upper limits obtained by Songaila et al. (1994a, 1994b). The filled square is obtained here. The filled hexagon is obtained by Lu et al. (1996).

temperature of the C I ground-state fine-structure levels at  $z \sim 2$  in reasonable physical and chemical conditions for C I to exist. After estimating these local contributions, our best guess for the CMBR temperature is  $7.9 \pm 1.0$  K, which is consistent with the predicted value of 8.105 K at  $z = 1.9731$ .

Our study shows that the local contributions to the excitation of the C I fine-structure levels are dominated by collisions with neutral hydrogen and UV pumping. However, if the number density of molecular hydrogen is comparable to that of neutral hydrogen,  $H_2$  can also be an important collisional partner for C I excitation. At high electron temperature (i.e., 1000 K or higher) electrons can also be important collisional partners.

Our study also shows that the UV radiation field in the

$z = 1.9731$  absorber is about 10 times stronger than the average value in the Milky Way. This could be the result of a higher star formation rate in this system.

Figure 6 illustrates the measurements of the CMBR temperature at different redshifts. All high-redshift measures are essentially upper limits since local contributions to the C I and C II excitation may be significant. So far, all measurements are consistent with the big bang predictions.

We thank A. Songaila for pointing out an important point which improved the paper. We thank G. Ferland for providing his CLOUDY program. We also thank the staff of MMT0 for their help. This research was supported by NSF AST 90-58510 and NASA grant NAGW-2201.

#### REFERENCES

- Bahcall, J. N., Joss, P. C., & Lynds, R. 1973, *ApJ*, 182, L95  
 Bahcall, J. N., & Wolf, R. A. 1968, *ApJ*, 152, 701  
 Bechtold, J. 1994, *ApJS*, 91, 1  
 Black, J. H. 1987, in *Interstellar Processes*, ed. D. J. Hollenbach & H. A. Thronson, Jr. (Dordrecht: Reidel), 931  
 Ferland, G. J. 1993, Dept. Phys. & Astron. Internal Rep., Univ. Kentucky  
 Flower, D. 1990, *Molecular Collisions in the Interstellar Medium* (Cambridge: Cambridge Univ. Press)  
 Jenkins, E. B. 1986, *ApJ*, 304, 739  
 Jenkins, E. B., & Shaya, E. J. 1979, *ApJ*, 231, 55  
 Johnson, C. T., Burke, P. G., & Kingston, A. E. 1987, *J. Phys. B*, 20, 2553  
 Keenan, F. P., Lennon, D. J., Johnson, C. T., & Kingston, A. E. 1986, *MNRAS*, 220, 571  
 Launay, J. M., & Roueff, E. 1977, *A&A*, 56, 289  
 Lu, L., Sargent, W. L. W., Womble, D. S., & Barlow, T. A. 1996, *ApJ*, 457, L1  
 Mather, J. C., et al. 1994, *ApJ*, 420, 439  
 Mathis, J. S., Mezger, P. G., & Panagia, N. 1983, *A&A*, 128, 212  
 Meyer, D. M., Black, J. H., Chaffee, F. H., Foltz, C. B., & York, D. G. 1986, *ApJ*, 308, L37  
 Morton, D. C. 1991, *ApJS*, 77, 119  
 Peebles, P. J. E. 1993, *Principles of Physical Cosmology* (Princeton: Princeton Univ. Press)  
 Pettini, M., Smith, L. J., Hunstead, R. W., & King, D. L. 1994, *ApJ*, 426, 79  
 Roueff, E., & Le Bourlet, J. 1990, *A&A*, 236, 515  
 Schneider, D. P., et al. 1993, *ApJS*, 87, 45  
 Schröder, K., Staemmler, V., Smith, M. D., Flower, D. R., & Jaquet, R. 1991, *J. Phys. B*, 24, 2487  
 Songaila, A., et al. 1994a, *Nature*, 368, 599  
 ———. 1994b, *Nature*, 371, 43  
 Staemmler, V., & Flower, D. R. 1991, *J. Phys. B*, 24, 2343